Recent advances in EUV phase-shifting point diffraction interferometry

Patrick Naulleau[a], Kenneth A. Goldberg[a], Sang H. Lee[a, b], Chang Chang[a, b], Phillip Batson[a], David Attwood[a, b], and Jeffrey Bokor[a, b]

[a] Center for X-Ray Optics, Lawrence Berkeley National Laboratory, Berkeley, CA 94720
[b] EECS Department, University of California, Berkeley, CA 94720

ABSTRACT

The extreme ultraviolet (EUV) phase-shifting point diffraction interferometer (PS/PDI) was developed and implemented at Lawrence Berkeley National Laboratory to meet the significant measurement challenge of characterizing EUV projection lithography optics. The PS/PDI has been in continuous use and under ongoing development since 1996. Here we describe recent improvements made to the interferometer, and we summarize metrology results from state-of-the-art 10×-reduction EUV projection optics.

Keywords: interferometry, point-diffraction interferometry, extreme ultraviolet lithography

1. INTRODUCTION

The semiconductor industry's push towards ever-smaller circuit feature sizes has led to a continual shortening of the wavelength used in the lithography step. Lithography systems used in mass production have historically been based on refractive projection optical systems. However, continuation of the wavelength-shortening trend will eventually lead to a departure from refractive systems. One of the most promising so-called *next-generation lithography* systems is extreme ultraviolet (EUV) projection lithography, in which multilayer-coated mirrors are used to form compound projection optics operating in the 11- to 14-nm-wavelength range. Achieving lithographic-quality, diffraction-limited performance requires that the projection optics have rms wavefront quality on the order of $\lambda/50$ (0.27 nm at $\lambda = 13.4$ nm).[1] Reduction of flare from scattering in the EUV optics also poses important fabrication and metrology challenges. Because EUV systems utilize resonant reflective coatings,[2] at-wavelength characterization[3] is critical to the development process.

Various at-wavelength interferometric measurement techniques, including lateral-shearing interferometry[4] and Foucault and Ronchi testing,[5] have been reported. These methods, however, have yet to demonstrate the accuracy required for the development of EUV lithographic imaging systems. While the accuracy of interferometry is often limited by the quality of a reference element, a high-accuracy class of interferometers exists in which the reference wave is created by diffraction from a small aperture.[6-9]

In order to meet the at-wavelength wavefront metrology challenge, an EUV-compatible diffraction-class interferometer, the phase-shifting point diffraction interferometer (PS/PDI), was developed by Medecki *et al.*[10] The PS/PDI is a common-path, system-level interferometer that relies on pinhole diffraction to generate both the illumination and reference beams. A diffraction grating is used as the beam-splitting and phase-shifting element. The PS/PDI has recently been demonstrated to have a reference wavefront accuracy of better than $\lambda_{EUV}/350$ (0.4 Å) within a numerical aperture (NA) of 0.082.[11]

Another important, newly realized capability of the PS/PDI is an extended spatial-frequency measurement range, which allows the interferometer to be used to characterize flare.[12] This capability also enables the interferometer to be used for the qualification of profilometry- and scatterometry-based flare measurement techniques.[13]

Here we give an overview of the PS/PDI and its capabilities, and we present results from recent characterizations of prototype EUV lithographic imaging systems.

Downloaded From: http://proceedings.spiedigitallibrary.org/ on 03/27/2015 Terms of Use: http://spiedl.org/terms

2. PS/PDI DESCRIPTION

The PS/PDI is briefly described here; more complete descriptions have been previously published.[10,14,15] The PS/PDI is a variation of the conventional point diffraction interferometer[6,7] in which a transmission grating has been added to greatly improve the optical throughput of the system and to add phase-shifting capability. In the PS/PDI (Fig. 1), the optical system under test is coherently illuminated by a spherical wave generated by diffraction from a pinhole placed in the object plane. To guarantee the quality of the spherical-wave illumination, the pinhole diameter is chosen to be smaller than the resolution limit of the optical system. A grating placed either before or after the test optic is used to split the illuminating beam, creating the requisite test and reference beams. A mask (the *PS/PDI mask* in Fig. 1) is placed in the image plane of the test optic to block unwanted diffracted orders generated by the grating. The mask also serves to spatially filter the reference beam using a second pinhole (the *reference pinhole*), thereby, removing the aberrations imparted by the optical system. The test beam, which also contains the aberrations imparted by the optical system, is largely undisturbed by the image-plane mask: it passes through a window in the PS/PDI mask that is large relative to the diameter of the optical system point-spread function (PSF). The test and reference beams propagate to the mixing plane where they overlap to create an interference pattern recorded on a CCD detector. The recorded interferogram yields information on the deviation of the test beam from the nominally spherical reference beam.

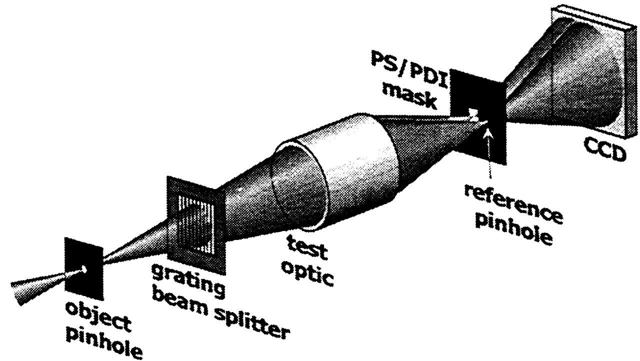

Fig. 1. Schematic of the phase-shifting point diffraction interferometer (PS/PDI).

3. CHARACTERIZING ACCURACY

Significant effort has been directed toward characterizing the accuracy of the PS/PDI.[11,16] The two primary sources of measurement error that limit the accuracy of the PS/PDI are imperfections in the reference wave generated by diffraction from the image-plane pinhole, and systematic effects that arise from the geometry of the system. Noting that the systematic geometric effects can be removed, provided they can be measured, the accuracy of the PS/PDI is typically limited by the reference-pinhole-induced errors.

In order to characterize the errors described above, and hence calibrate the PS/PDI, null tests have been performed. Analogous to Young's two-slit experiment, a null test can be performed on the PS/PDI by replacing the image-plane window with a second reference pinhole. In the null-test case, two reference waves are generated by diffraction from the image-plane mask, creating a fringe pattern (interferogram) in the far field of the mask. Aberrations calculated from the interferogram are indicative of the systematic and random errors in the interferometer.

Implementation of this test shows the primary error to result from the hyperbolic fringe pattern produced by the two, laterally displaced, nominally spherical waves. Because this error is easily predicted, measured, and subtracted during analysis,[15] we consider the reference-wavefront-limited accuracy to be the residual null-test wavefront error after its removal.

Table 1. Reference wave rms accuracy as a function of null-mask pinhole size.

Pinhole Size (nm)	Systematic-error-limited rms accuracy (waves)
140	0.012 ± 0.001 (0.16 nm or λ/83)
120	0.010 ± 0.001 (0.14 nm or λ/100)
100	0.0041 ± 0.0003 (0.055 nm or λ/244)
80	0.0028 ± 0.0001 (0.038 nm or λ/357)

Table 1 enumerates the null-test-measured

Downloaded From: http://proceedings.spiedigitallibrary.org/ on 03/27/2015 Terms of Use: http://spiedl.org/terms

systematic-error-limited accuracy as a function of pinhole size. The accuracy quoted spans a NA of 0.082; the image-side NA of the optic used for this test was 0.08. As expected, the reference-wavefront accuracy improves with a reduction in pinhole size, and a resultant improvement in spatial filtering. Figure 2 shows a typical null-test interferogram using 100-nm-diameter pinholes and a wavelength of 13.5 nm.

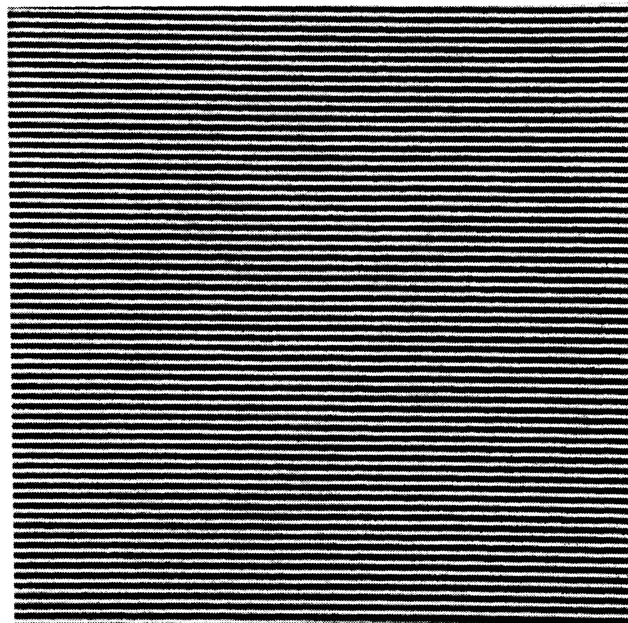

Fig. 2. Representative null-test interferogram using 100-nm pinholes (λ = 13.5 nm).

This and other measurements described here were performed using an undulator beamline[17] at the Advanced Light Source synchrotron radiation facility at Lawrence Berkeley National Laboratory. The beamline provides a tunable source of EUV radiation with a coherence area that is significantly larger than the 0.75-μm diameter object-plane pinhole.[18] All tests were performed at the wavelength matching the peak reflectivity wavelength of the optic under test.

Experiments reveal that the quality of the reference wavefront is limited by incomplete spatial filtering of the aberrated wavefront produced by the optic under test, not by physical pinhole diffraction limits of planar waves.[19] Depending on the pinhole size, this incomplete spatial filtering is due to residual transmission through the membrane or aberrations passing through the finite sized pinhole. One significant consequence of this property is the prediction that measurement accuracy will improve with improvement in the quality of the optic under test. The optic used in these measurements has an EUV wavefront quality of 0.16 waves rms over a NA of 0.08, whereas current state-of-the-art optics[20] have been measured to have wavefront aberrations below 0.05 waves rms over a slightly larger NA.[21] Although not yet verified with subsequent null tests, the accuracy obtained when testing these newer optics is expected to be better than the results presented in Table 1.

4. OPTIMIZING CONTRAST

A possible source of error not measured by the null test described above is wavefront error induced by the grating beam splitter. Line-placement errors in the grating are mapped to wavefront errors in the diffracted wavefront. Because the undiffracted beam (the zero order of the grating) is immune to these errors, the PS/PDI has typically been implemented using the zero order as the test beam and the first-diffracted order as the reference beam. In this configuration (the *first-order-reference* configuration), aberrations imparted by grating line-placement errors are filtered by the reference pinhole. A drawback of this configuration, however, is that it leads to low fringe contrasts when small pinholes are used or large aberrations are present. This problem is a consequence of the amplitude transmission gratings currently used in the EUV PS/PDI. With amplitude gratings, this configuration can at best provide a one-to-one reference-to-test-beam power ratio as defined prior to the filtering loss induced by the image-plane pinhole. When high accuracy is sought and small pinholes are used, this filtering loss becomes significant, leading to a large power mismatch between the two beams. The same is also true when the test optic contains large aberrations leading to a large PSF. Power mismatch between the test and reference beams yields interferograms of low contrast that are susceptible to noise, including photon, detector-quantization, and other camera noise terms. Therefore, the power mismatch places practical limits on the minimum pinhole size, and the size of the aberrations that can be measured in the first-order-reference configuration.

Assuming grating-line-placement errors are smaller than the reference-pinhole-induced errors for the contrast-limited pinhole size, it is beneficial to reverse the beams used as the reference and test waves. In this

Downloaded From: http://proceedings.spiedigitallibrary.org/ on 03/27/2015 Terms of Use: http://spiedl.org/terms

zero-order-reference configuration, arbitrarily high reference-to-test-beam power ratios can be achieved by using binary gratings with duty-cycles other than 50%, allowing arbitrarily small reference pinholes to be used. The grating duty cycle can, in principle, be chosen to exactly balance the filtering loss, which depends both on the aberrations in the test optic and on the size of the reference pinhole. This zero-order-reference configuration is now routinely used when testing optics, enabling the use of 100-nm and smaller reference pinholes. Measurements have shown the grating-induced error in the zero-order-reference configuration to be approximately $\lambda/330$ (the gratings used were fabricated by electron-beam lithography). Assuming these line-placement errors are uncorrelated over large displacements of the grating, the effective grating-limited accuracy can be further improved through an averaging process.

5. ELIMINATING SCATTERED-REFERENCE-LIGHT CORRUPTION

Another problem that arises when small reference pinholes are used is scattered-reference-light corruption. Because the PS/PDI derives its reference beam by spatial filtering a laterally displaced copy of the test beam, mid- to high-spatial-frequency features in the optic under test will scatter reference-beam light through the image-plane test window. In the presence of this scattered reference light, the reference beam is no longer a clean spherical wave, but includes high-frequency features that contaminate the measurement. Because the pinhole size affects the power in the spatially filtered component of the reference beam, but does not change the power of the reference light scattered through the test window, the scattered-light contamination problem becomes more significant as smaller pinholes are used.

When conventional phase-shifting data-acquisition and time-domain analysis methods[22,23] are used, the scattered reference light interfering with the test beam is indistinguishable from the pinhole-diffracted reference light interfering with the test beam. As an alternative to the phase-shifting method, the PS/PDI spatial carrier makes it possible to use spatial-domain interferogram analysis techniques such as the Fourier-transform method.[24] This method, however, also suffers in the presence scattered-reference-light contamination: in this case, the problem is caused by scattered reference light interfering with the pinhole-diffracted reference light. In both these cases, the unwanted interference terms lead to difficulties in performing the phase unwrapping and to inaccuracies in the determination of mid-spatial-frequency components of the reconstructed wavefront.

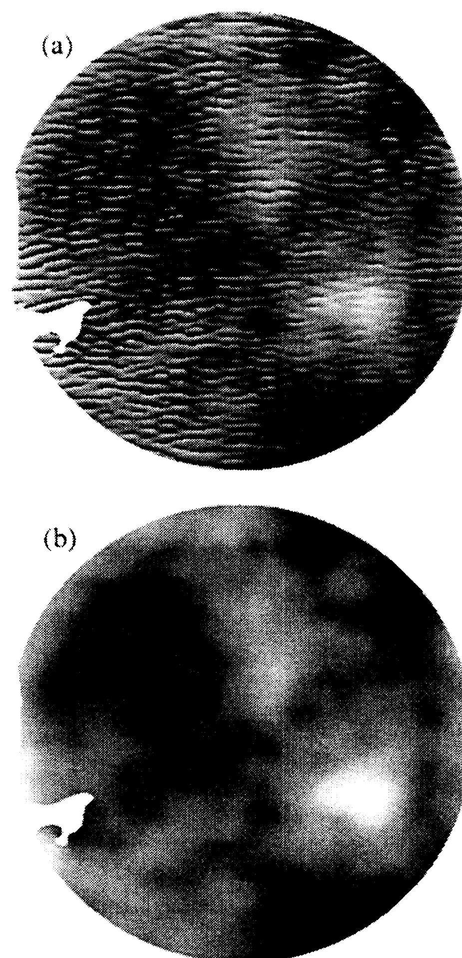

Fig. 3. Wavefront obtained using (a) standard temporal-processing (phase-shifting) technique and (b) using the dual-domain method. Same source data was used in both cases. The masked regions of the wavefront are the edge of the aperture and areas where the test optic reflectance was too low to accurately measure the phase. The high-frequency features in (a) are caused by the scattered-reference-light corruption.

Recently, a *dual-domain* technique[25] capable of eliminating scattered-reference-light corruption has been demonstrated. The dual-domain method is essentially a three-tiered filtering system composed of lowpass spatial-filtering the test-beam electric field, bandpass spatial-filtering the individual interferogram irradiance frames of a phase-shifting series, and bandpass temporal-filtering the phase-shifting series as a whole. The first step is physical and is performed by the test-beam window, whereas the last two steps are implemented numerically.

Downloaded From: http://proceedings.spiedigitallibrary.org/ on 03/27/2015 Terms of Use: http://spiedl.org/terms

The effectiveness of this technique is demonstrated in Fig. 3. The test optic is the same objective used for the null test described above, and the reference pinhole size is 100 nm. Figure 3(a) shows the wavefront obtained using standard temporal-processing (phase-shifting) techniques. The *masked* regions of the wavefront are the edge of the aperture and areas where the test-optic reflectance was too low to accurately measure the phase. The high-frequency features in Fig. 3(a) can be attributed to scattered-reference-light corruption. In Fig. 3(b) we see the results for the same data set analyzed using the dual-domain method. The scattered-reference-light noise has been effectively suppressed. The rms wavefront error for the dual-domain processing result is 2.13 nm (0.16 waves), whereas the wavefront error is 2.72 nm (0.20 waves) using the conventional temporal-domain method. The rms magnitude of the difference wavefront between Figs. 3(a) and 3(b) is 1.68 nm (0.13 waves).

6. MEASURING FLARE

The original design of the PS/PDI was primarily directed towards high-accuracy wavefront characterization. For lithographic printing, however, it is equally important to consider flare. Flare is the *halo* of light surrounding the optical system PSF, caused by scatter from within the optical system. The capabilities of the PS/PDI have recently been extended, allowing it to measure both wavefront and flare simultaneously.[12] This new capability is a direct consequence of the dual-domain method described above. The PS/PDI-based flare measurement technique has advantages over flare measurement techniques based on roughness characterization of individual optical components[13] because it is an integrated system measurement performed at the operational wavelength. Moreover, the interferometric method requires no additional data collection beyond the data currently collected for EUV wavefront metrology.

Because PS/PDI-based wavefront metrology measures the wavefront at the exit pupil of the optical system, it is equivalent to PSF metrology (the two form a Fourier-transform pair). For this reason, the flare can be characterized using wavefront metrology data if it contains enough spatial-frequency bandwidth. In particular, the mid-spatial-frequency range falling between the ranges commonly referred to as figure and finish, is important for flare determination.

The measurement bandwidth of the PS/PDI is simply determined by the size of the image-plane test window. Consequently, the area over which the scattered light can be measured in the image plane is the area of the test window. Using the dual-domain method to provide an accurate measure of the mid-spatial-frequency range, and using elongated windows to extend the measured range, it is possible to characterize flare with the PS/PDI.

The PS/PDI-based flare measurement technique has been demonstrated[12] using a recently fabricated (1998) EUV optical system developed to meet a figure specification of better than 0.8 nm and flare specification of less than 5% in a 4-μm line.[20,21] The measurements were performed using 30×3 μm image-plane windows. The narrow window size in the direction of the beam separation is a requirement of the dual-domain method.[25]

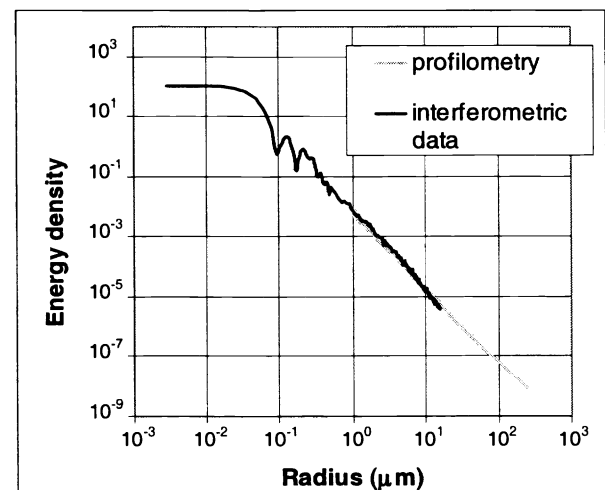

Fig. 4. Comparison of the scatter-energy density as a function of radial separation from the PSF peak determined by the PS/PDI- and profilometry-based methods respectively. The relationship between radial distance in the image plane and spatial frequencies on the optical components is 3 mm^{-1} per μm for the primary and 0.55 mm^{-1} per μm for the secondary.

From the measured PSF, the normalized scatter-energy density as a function of radial distance from the PSF peak can be found. This is simply the radially averaged PSF. Anisotropic scattering effects are

Downloaded From: http://proceedings.spiedigitallibrary.org/ on 03/27/2015 Terms of Use: http://spiedl.org/terms

investigated by repeating the measurement with a 90-degree rotation of the test window. Combining the results from the measurements performed in the two orthogonal directions yields the scatter energy depicted in Fig. 4. The imperfect Airy lobes are caused by aberrations in the optic (figure error).

To predict the flare expected in a typical imaging situation, the scatter-energy density must be known over the full radial extent of the field. For the optics considered here, the full field size is 250-μm radius in the image plane. The extended-range scatter-energy density can be obtained by extrapolation of the interferometrically determined data or by use of data derived from profilometry performed on the individual substrates before assembly of the optical system.[26] In order to avoid possible extrapolation errors, we choose the latter. The plot in Fig. 4 shows an overlay of the scatter-energy density predicted from profilometry onto the PS/PDI-based measurement. The two measurement methods have overlapping data in the radial range from 1 μm to 16 μm. Good agreement between the two methods is evident. The flare in an arbitrary feature may be calculated from the scatter-energy density. Considering an isolated, dark 4-μm line in a 250-μm-radius bright field, the flare is calculated to be 3.9%. For this optic, the flare value predicted by profilometry alone is 4.0%.[26]

7. CHARACTERIZATION OF THREE NEW EUV OPTICS

During the past year, three new 10×-reduction EUV Schwarzschild cameras[27] have been characterized with the EUV PS/PDI. Furthermore, two of the cameras underwent at-wavelength alignment, significantly improving the system wavefronts.[28] All three cameras were fabricated to the same optical design specifications and were built within the past two years. The optics have an image-side NA of 0.088 and utilize molybdenum/silicon multilayer coatings designed for peak reflectivity at 13.4 nm wavelength.

Based on fitting to the first-37 Zernike polynomial terms,[29] the rms wavefront error magnitudes (σ) for Cameras labeled B1, B2 and A are 0.62 nm (0.046 waves), 0.52 nm (0.039 waves), and 0.99 nm (0.074 waves), respectively, within 0.088 NA. EUV alignment was performed on Cameras B2 and A. The measured wavefronts are shown in Fig. 5.

Because the wavefront aberrations in these systems vary as a function of field-point position,[21] accurate selection of the field point used to perform the measurements is important. The conjugate accuracy is particularly important when comparing EUV PS/PDI metrology to other methods, such as the visible-light phase-shifting

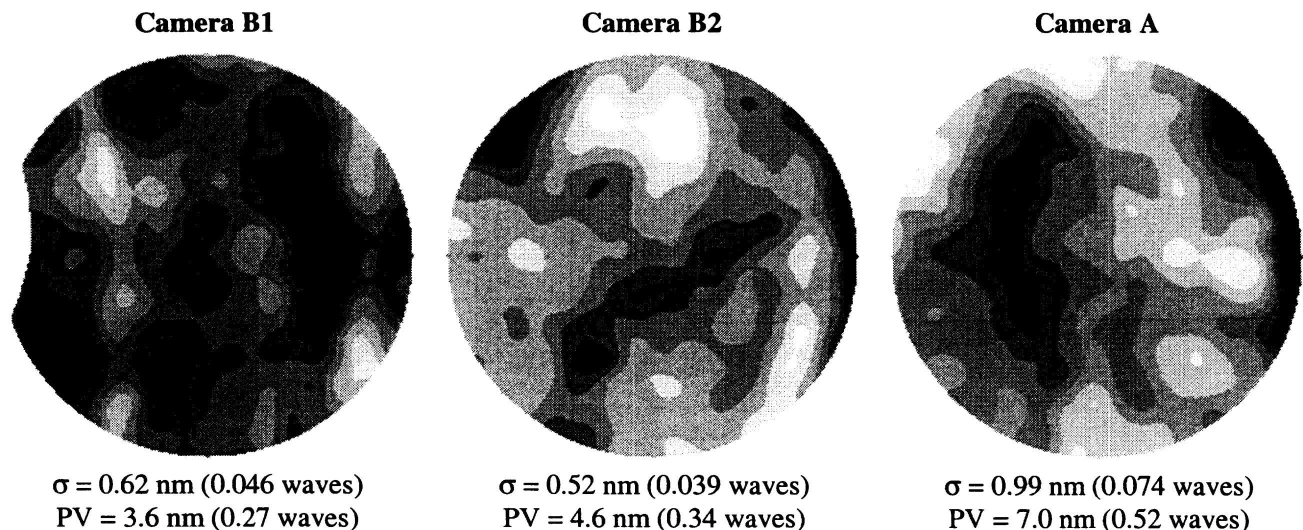

Fig. 5. PS/PDI-measured wavefronts of three recently fabricated 10×-reduction EUV Schwarzschild cameras. The wavefront statistics are quoted over an NA of 0.088, and are based on 37-term Zernike fitting. The displayed wavefronts, however, include higher spatial frequency features. The displayed wavefronts are individually scaled. The measurement wavelength was 13.4 nm.

Downloaded From: http://proceedings.spiedigitallibrary.org/ on 03/27/2015 Terms of Use: http://spiedl.org/terms

diffraction interferometer developed at Lawrence Livermore National Laboratory,[8,9] and when predicting imaging performance. To address this issue, a kinematic object-point-alignment fixture has been fabricated for the PS/PDI. Used in conjunction with a similar fixture fabricated for the visible-light phase-shifting diffraction interferometer, this object-point-alignment tool has enabled detailed and favorable comparisons of visible-light and EUV metrology.[21]

In addition to the extremely high accuracy provided by the EUV PS/PDI, its ability to measure chromatic wavefront effects makes it an important tool for characterizing EUV lithographic optics. Because visible light interacts primarily with the top surface of multilayer reflective coatings, visible light interferometry is incapable of distinguishing between substrate features and coating effects. EUV interferometry, on the other hand, utilizes the operational wavelength to measure the system wavefront and, hence, can separate substrate from coating effects by probing the system wavefront as a function of wavelength.

Figure 6 shows the measured wavefront, rms wavefront error (σ), and peak-to-valley wavefront error (PV) as a function of wavelength for Camera A. The wavefront statistics are based on an NA of 0.087 and include the full measured spatial-frequency bandwidth. The discrepancy in wavefront statistics compared to the Camera A value in Fig. 5 is due to the slightly smaller NA in Fig. 6. Also shown in Fig. 6 are the difference wavefronts with respect to the passband-center wavelength of 13.4 nm. The measurements were taken at 0.1-nm intervals from 13.1 to 13.8 nm, extending beyond the measured transmittance bandwidth of the optic.

The extremely small chromatic effects are indicative of the high-quality coatings that are now available.[30,31] These coatings are significantly better than those from previously studied[32] optics fabricated about four years

λ (σ) [PV] nm	Wavefront	Wavefront difference from λ=13.4 nm	λ (σ) [PV] nm
13.1 (0.857) [5.37]			**13.1** (0.031) [0.36]
13.2 (0.860) [5.45]			**13.2** (0.015) [0.20]
13.3 (0.865) [5.47]			**13.3** (0.008) [0.08]
13.4 (0.869) [5.46]			**13.4** (0.000) [0.00]
13.5 (0.875) [5.48]			**13.5** (0.012) [0.07]
13.6 (0.887) [5.55]			**13.6** (0.033) [0.16]
13.7 (0.898) [5.61]			**13.7** (0.046) [0.26]
13.8 (0.903) [5.67]			**13.8** (0.052) [0.36]

Fig. 6. The first column of images is the measured wavefront for Camera 3 as a function of wavelength with the focus nulled at 13.4 nm. The second column of images shows the difference wavefront for all the wavefronts compared to the 13.4-nm wavefront. Also shown are the rms (σ) and peak-to-valley (PV) wavefront errors for each case. Each column is displayed on a global color scale. In the first column, the peak-to-valley is 5.69 nm and each color contour represents 0.38 nm. In the second column, the peak-to-valley of the set of difference wavefronts is 0.48 nm whereas the color scale is set to a peak-to-valley of 0.29 nm in order to better accentuate the features, each color contour represents 0.019 nm.

Downloaded From: http://proceedings.spiedigitallibrary.org/ on 03/27/2015 Terms of Use: http://spiedl.org/terms

ago. In the older optics, the coating-induced peak-to-valley wavefront magnitude changes were as large as 6 nm compared the smaller than 0.4-nm effects seen here.

8. CONCLUSION

The past year has seen significant advances in the EUV PS/PDI and in the development of high-quality 10×-reduction EUV projection optics. The PS/PDI has a demonstrated reference-wavefront accuracy of better than $\lambda_{EUV}/350$. The robustness, dynamic range, and noise immunity of the PS/PDI has been enhanced through the development of high-contrast configurations and the dual-domain data-acquisition and processing technique. The measurement bandwidth of the PS/PDI has been extended considerably, allowing it to be used to characterize flare as well as wavefront errors. Finally, the PS/PDI has been instrumental in the development of state-of-the-art EUV projection systems with rms wavefront errors as low as 0.52 nm (0.039 waves).

ACKNOWLEDGEMENTS

The authors are greatly indebted to Hector Medecki and Edita Tejnil for their pivotal roles in the early development of the PS/PDI. We are also grateful to Erik Anderson for nanofabrication of pinholes and gratings, and to the entire CXRO staff including Bill Bates, Rene Delano, Keith Jackson, Gideon Jones, Drew Kemp, David Richardson, and Senajith Rekewa for facilitating this research. Special thanks are due to Paul Denham for expert assistance with experimental control systems. This research was supported by the Extreme Ultraviolet Limited Liability Company, the Semiconductor Research Corporation, DARPA Advanced Lithography Program, and the Department of Energy Office of Basic Energy Science.

REFERENCES

1. D. M. Williamson, "The elusive diffraction limit," *OSA Proceedings on Extreme Ultraviolet Lithography*, F. Zernike and D. T Attwood, eds. (Optical Society of America, Washington, DC 1995), Vol. 23, pp. 68-76.
2. J. H Underwood and T. W. Barbee, Jr., "Layered synthetic microstructures as Bragg diffractors for X rays and extreme ultraviolet: theory and predicted performance," Appl. Opt., **20**, 3027-3034 (1981).
3. D. Attwood, G. Sommargren, R. Beguiristain, K. Nguyen, J. Bokor, N. Ceglio, K. Jackson, M. Koike, and J. Underwood, "Undulator radiation for at-wavelength interferometry of optics for extreme-ultraviolet lithography," Appl. Opt., **32**, 7022-7031 (1993).
4. J. E. Bjorkholm, A. A. MacDowell, O. R. Wood II, Z. Tan, B. LaFontaine, and D. M. Tennant, "Phase-measuring interferometry using extreme ultraviolet radiation," J. Vac. Sci. & Technol. B, **13**, 2919-2922 (1995).
5. A. K. Ray-Chaudhuri, W. Ng, F. Cerrina, Z. Tan, J. Bjorkholm, D. Tennant, and S. J. Spector, "Alignment of a multilayer-coated imaging system using extreme ultraviolet Foucault and Ronchi interferometric testing," J. Vac. Sci. Technol. B, **13**, 3089-3093 (1995).
6. W. Linnik, "A simple interferometer to test optical systems," Proceedings of the Academy of Science of the USSR, **1**, 210-212 (1933).
7. R. N. Smartt and W. H. Steel, "Theory and application of point-diffraction interferometers," Jap. J. Appl. Phys., **14**, Suppl.14-1, 351-356 (1975).
8. G. E. Sommargren, "Phase shifting diffraction interferometry for measuring extreme ultraviolet optics," OSA Trends in Optics and Photonics Vol. 4, Extreme Ultraviolet Lithography, G.D. Kubiak and D.R. Kania, eds. (Optical Society of America, Washington, DC 1996), pp. 108-112.
9. G. E. Sommargren, "Diffraction methods raise interferometer accuracy," Laser Focus World, **32**, 61-71 (1996).
10. H. Medecki, E. Tejnil, K. A. Goldberg, and J. Bokor, "Phase-shifting point diffraction interferometer," Opt. Lett., **21**, 1526-1528 (1996).

Downloaded From: http://proceedings.spiedigitallibrary.org/ on 03/27/2015 Terms of Use: http://spiedl.org/terms

11. P. Naulleau, K. A. Goldberg, S. Lee, C. Chang, D. Attwood, and J. Bokor, "The EUV phase-shifting point diffraction interferometer: a sub-angstrom reference-wave accuracy wavefront metrology tool," *submitted to Appl. Opt.* (5/99).
12. P. Naulleau, K. A. Goldberg, E. Gullikson, and J. Bokor, "Interferometric at-wavelength flare characterization of EUV optical systems," *submitted to J. Vac. Sci. & Technol. B* (6/99).
13. E. M. Gullikson, "Scattering from normal incidence EUV optics," in *Emerging Lithographic Technologies II*, Yuli Vladimirski, ed., Proc. SPIE, **3331**, 72-80, (1998).
14. E. Tejnil, K. A. Goldberg, S. H. Lee, H. Medecki, P. J. Batson, P. E. Denham, A. A. MacDowell, J. Bokor, and D. Attwood, "At-wavelength interferometry for EUV lithography," J. Vac. Sci. & Technol. B, **15**, 2455-2461 (1997).
15. K. A. Goldberg, "Extreme Ultraviolet Interferometry," Ph.D. dissertation (University of California, Berkeley, 1997).
16. P. Naulleau, K. A. Goldberg, S. Lee, C. Chang, C. Bresloff , P. Batson, D. Attwood, and J. Bokor, "Characterization of the accuracy of EUV phase-shifting point diffraction interferometry," in *Emerging Lithographic Technologies II*, Yuli Vladimirski, ed., Proc. SPIE **3331**, 114-123 (1998).
17. R. Beguiristain, J. Underwood, M. Koike, P. Batson, E. Gullikson, K. Jackson, H. Medecki, and D. Attwood, "High flux undulator beam line optics for EUV interferometry and photoemission microscopy," in *High Heat Flux Engineering III*, A. M. Khounsary, ed., Proc. SPIE **2855**, 159-169 (1996).
18. D. Attwood, P. Naulleau, K. Goldberg, E. Tejnil, C. Chang, R. Beguiristain, P. Batson, J. Bokor, E. Gullikson, M. Koike, H. Medecki, and J. Underwood, "Tunable coherent radiation in the soft X-ray and extreme ultraviolet spectral regions," IEEE J. Quantum Electron, **35**, 709-720 (1999).
19. K. A. Goldberg, et al., "A 3-D numerical study of pinhole diffraction to predict the accuracy of EUV point diffraction interferometry," *OSA Trends in Optics and Photonics*, Optical Society of America, Washington, D.C., **4**, 133-137 (1996).
20. J. Goldsmith, K. Berger, D. Bozman, G. Cardinale, D. Folk, C. Henderson, D. O'Connell, A. Ray-Chaudhuri, K. Stewart, D. Tichenor, H. Chapman, R. Gaughan, R. Hudyma, C. Montcalm, E. Spiller,J. Taylor, J. Williams, K. Goldberg, E. Gullikson, P. Naulleau, J. Cobb, "Sub-100-nm imaging with the EUV 10× Microstepper," in Emerging Lithographic Technologies III, Y. Vladimirski, ed., Proc. SPIE, **3676**, *to be published* (1999).
21. K. A. Goldberg, P. Naulleau, R. Gaughan, H. Chapman, J. Goldsmith, and J. Bokor, "Direct comparison of EUV and visible-light interferometries," in Emerging Lithographic Technologies III, Y. Vladimirski, ed., Proc. SPIE, **3676**, *to be published* (1999).
22. R. Crane, "Interference phase measurement," Appl. Opt., **8**, 538-542 (1969).
23. J. H. Bruning, D. R. Herriot, J. E. Gallagher, D. P. Rosenfeld, A. D. White, and D. J. Brangaccio, "Digital wavefront measuring interferometer for testing optical surfaces and lenses," Appl. Opt., **13**, 2693-2703 (1974).
24. M. Takeda, H. Ina, and S. Kobayashi, "Fourier-transform method of fringe-pattern analysis for computer-based topography and interferometry," J. Opt. Soc. Am., **72**, 156-160 (1982).
25. P. Naulleau and K. A. Goldberg, "Dual-domain point diffraction interferometer," Appl. Opt, **38**, 3523-3533 (1999).
26. E. Gullikson, S. Baker, J. Bjorkholm, J. Bokor, K. Goldberg, J. Goldsmith, C. Montcalm, P. Naulleau, E. Spiller, D. Stearns, J. Taylor, and J. Underwood, "EUV scattering and flare from 10× projection cameras," in Emerging Lithographic Technologies III, Y. Vladimirski, ed., Proc. SPIE, **3676**, *to be published* (1999).
27. D. A. Tichenor, G. D. Kubiak, M. E. Malinowski, R. H. Stulen, S. J. Haney, K. W. Berger, R. P. Nissen, R. L. Schmitt, G. A. Wilkerson, L. A. Brown, P. A. Spence, P. S. Jin, W. C. Sweat, W. W. Chow, J. E. Bjorkholm, R. R. Freeman, M. D. Himel, A. A. MacDowell, D. M. Tennant, O. R. Wood II, W. K. Waskiewicz, D. L. White, D. L. Windt, and T. E. Jewell, "Development and characterization of a 10× Schwarzschild system for SXPL," in *OSA Proceedings on Soft X-Ray Projection Lithography,* Vol. 18, A. M. Hawryluk and R. H. Stulen, eds., (Optical Society of America, Washington, DC, 1993), pp. 79-82.

Downloaded From: http://proceedings.spiedigitallibrary.org/ on 03/27/2015 Terms of Use: http://spiedl.org/terms

28. K. A. Goldberg, P. Naulleau, and J. Bokor, "EUV interferometric measurements of diffraction-limited optics," *submitted to J. Vac. Sci. & Technol. B* (6/99).
29. A. Bathia and E. Wolf, "The Zernike circle polynomials occurring in diffraction theory," Proc. Phys. Soc., **B65**, 909-910 (1952).
30. E. Spiller, F. J. Weber, C. Montcalm, S. L. Baker, E. M. Gullikson, and J. H. Underwood, "Multilayer coating and tests of a 10X extreme ultraviolet lithography camera," in *Emerging Lithographic Technologies II*, Y. Vladimirski, ed., Proc. SPIE **3331**, 62-71 (1998).
31. C. Montcalm, S. Bajt, P. B. Mirkarimi, E. Spiller, F. J. Weber, and J. A. Folta, "Multilayer reflective coatings for extreme-ultraviolet lithography," in *Emerging Lithographic Technologies II*, Y. Vladimirski, ed., Proc. SPIE **3331**, 42-51 (1998).
32. E. Tejnil, K. A. Goldberg, and J. Bokor, "Phase Effects Owing to Multilayer Coatings in a Two-Mirror Extreme-Ultraviolet Schwarzschild Objective," Appl. Opt, **37**, 8021-8029 (1998).

Downloaded From: http://proceedings.spiedigitallibrary.org/ on 03/27/2015 Terms of Use: http://spiedl.org/terms